Broadband High-Efficiency 3-bit Coding Metasurface in Tramsmission Mode Based on the Polarization Conversion Technique

Majid Karimipour[1,*], Mohammad Bagher Heydari[2], and Iman Aryanian[3]

[1]Arak University of Technology, department of electrical engineering, Arak, +98, Iran
[2]Iran University of Science and Technology, Tehran, Iran, +98
[3]Iran Telecommunication Research Center (ITRC), Tehran, +98, Iran
[*]m.karimipour@arakut.ac.ir

ABSTRACT

The main drawback of the transmissive focusing metasurface (TFM) is its low operational bandwidth and low aperture efficiency which usually the simultaneous increase of these two radiation characteristics is a major challenge in these structures. This paper introduces a novel multi-state coding metasurface with an enhanced frequency bandwidth and efficiency exploiting system-level and element-level synthesis approaches. Unlike most of the TFMs proposed in this concern, the proposed novel element consists of only two dielectric layers. The system-level synthesis approach is implemented by the well-established broadband technique named multi-frequency phase synthesis (MFPS) using an optimization algorithm to balance the phase error in the whole band in terms of gain and aperture efficiency. At the element design level, a wideband technology based on the polarization conversion technique (PCT) is adopted and implemented by a subwavelength non-resonant element which is composed of three C-shape metallic patterns. The metal layers are printed on two sides of two identical dielectric layers without using any metalized via in the configuration. Eight states of phase quantization are realized by simply changing the angle of arc curves in all layers. The amplitude of the transmitted wave with rotated polarization is larger than 0.9 from 12.3 GHz to 16.5 GHz. A 25×25-element TFM is designed, fabricated, and tested by the above broadband technique. The measurement results demonstrate that the 1-dB gain bandwidth of the antenna is 12.3-16.5 GHz which is equal to 29%. The maximum measured aperture efficiency is 53.6%, which occurs at 12.8 GHz. The proposed metasurface is classified in the group of broadband high-efficiency TFM.

Introduction

Combining the advantages of parabolic and phased array radiators, a new class of high gain spatially-fed radiator in transmitting and reflecting modes is introduced which eliminates the complicated feeding network and consequently undesirable losses of the feeding structure thanks to the use of spatial feed system[1,2]. In comparison with reflecting focusing metasurface (RFM), TFM is a promising solution to omit the feed blockage effect since the feed and radiation pattern are on opposite sides of the metasurface while keeping other advantages such as low profile, low cost, ease of fabrication, and light weight. There are two main challenges to the design of a high-performance TFM. First, the working frequency bandwidth, which returns to the narrowband behavior of phasing elements. Second, the low aperture efficiency, which returns to the inherent insertion loss of the metasurfaces in the transmissive mode. The former challenge is common between the RFM and TFM while the latter one is more prominent in TFM than RFM. This is why, unlike the RFM, which can achieve high aperture efficiency even on single-layer configurations[3–5], high-efficiency TFMs are almost implemented by multi-layer metasurfaces[6–8]. In recent years, a lot of efforts have been done to enhance the bandwidth or aperture efficiency of TFMs[9–16]. All broadband approaches can be divided into three categories: (i) the use of multi-layer frequency selective surfaces[1,12,13], (ii) the use of sub-wavelength non-resonant unit cell and true-time-delay structures[14,15], and (iii) the use of receive/transmit approach using multi-layer configurations. The later one is also utilized in folded TFM configurations[16], in which at least three metallic layers is required for the phase and even polarization manipulation. In this regard, those elements that support two orthogonally polarized waves, such as V- or Y-shaped elements, have a much broader resonance compared with classical phasing elements[9].

Investigations show that few works have been done to improve the TFM bandwidth and aperture efficiency at the same time. For example, the authors in[9] used several combined broadband techniques to design an ultra-wideband configuration, however, the peak aperture efficiency is less than 50% since the element loss of all elements is not lower than -1 dB. Similarly, the study presented in[10] is a linearly polarized TFM based on a three-metallic phasing element reaching a peak aperture efficiency of 55%, however, the 1-dB gain bandwidth limits to 15.5%. The authors in[17] introduced a high-efficiency TFM based on the Huygens metasurface concept and reported 64% of aperture efficiency at the cost of a nearly difficult fabrication process. However, the 1-dB gain bandwidth of the proposed structure in[17] is only 14% which is not very high. Similar results are observed in[18]. Recently, a high gain dual polarized bulky 3-D full metal TFM has been introduced based on quadruple-ridged waveguide as the unit cell[19]. The measured peak aperture efficiency and 1-dB gain bandwidth are 41.9% and 27.3%, respectively, which is a relatively good achievement for these two specifications.

It is well-known that the phase quantization scheme is a favorable solution to the design of metasurface in reflection[20,21] and transmission[22] modes due to a simpler design process and featuring reconfigurable capabilities. We find out that the best solution to achieve a high-efficient broadband TFM is the use of coding structures with the phase quantization scheme. It is feasible to construct a well-behaved coding metasurface in terms of the amplitude and phase values of the transmission and reflection waves in a wide frequency region. This coding surface could be implemented by using a set of multi-degree-of-freedom elements to individually adopt proper dimensions for the geometry of the elements corresponding to each bit response. In doing so, two determinative factors named the low insertion loss and the required phase value, are considered during the proper selection of the element. These two factors ultimately guarantee the broadband and high-efficiency behavior of the metasurface.

In this paper, we aim to address the two aforementioned factors at the same time and develop a compact broadband high-efficiency TFM using a 3-bit coding metasurface. The main novelty of the proposed work compared with other previous coding metasurfaces is the use of both broadband techniques at the element and system design levels, integrating with a 3-bit metasurface which has a lower phase error than 1- and 2-bit configurations leading to enhancement the aperture efficiency. Not using the metalized via in the geometry of the element makes it possible to use it at millimeter wave frequencies and higher with the least possible error in its construction and assembly process in multi-layer configurations. Because at very high frequencies, the use of metallized via in structures will be one of the main factors of manufacturing errors[23].

Element Design

The proposed subwavelength unit cell is demonstrated in Fig. 1, which is properly designed based on multi-degree-of-freedom technology such that it fulfills the phase and amplitude requirements of all eight states of the 3-bit coding metasurface.

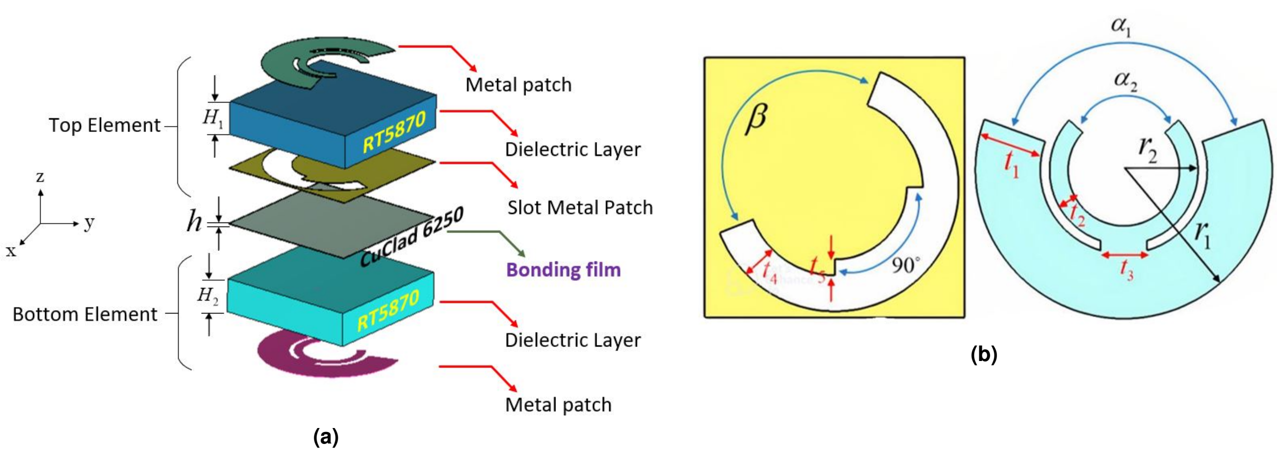

Figure 1. Geometry of the meta-atom. (a) The exploded view and (b) design parameters of the unit cell.

The unit cell, which is composed of three metallic layers, is designed based on the transmit/receive topology without any metallic via between the layers. The top and bottom metallic patterns are identical double C-shape patches with the thicknesses of t_1 and t_2 which are connected together with a narrow strip at the middle arc positions. The thickness of the strip is considered t_3. The opening angle of the arc section of the two C-shape patches is α_1 and α_2. The lower metallic layer of top element is a C-shape slot patch with the slot widths of t_4 and t_5. The optimum design parameters of the unit cell is listed in Table. 1. The unit cell dimensions is considered $6.5\ mm \times 6.5\ mm$ which is equal to $0.3\lambda_0$ at the center frequency of 14 GHz. The bottom and top dielectric layers are 1.57 mm-thickness of Rogers 5870 with $\varepsilon_r = 2.33$ and loss tangent of 0.0012. As shown in Fig. 1, the top and bottom elements are bonded to each other using a 0.038 mm thick thermoplastic bonding film (Cuclad 6250). By changing the opening angles of the patches and slot in all three metallic layers, the transmissive phase is manipulated. Thanks to the use of a sub-wavelength non-resonance structure, the element behavior is desirable in a wide frequency range in terms of magnitude and phase responses. Eight states for the transmissive phase to cover a full cycle of 360° is demonstrated in Fig. 2.

As it is clear in Fig. 2, when the desired phases are obtained for the first four states, i.e., the states of $1,2,3$, and 4, by tuning the α_1, α_2, and β parameters, the phase of other four states would simply be obtained by rotating the middle and bottom metal patch layers by 90° and 180° around the z-axis simultaneously. This possibility can be done due to the polarization conversion characteristic of the element in the transmission mode. Therefore, the design of 3-bit TFM working in polarization conversion mode requires determining only four states of phases for the unit cells. The simulated transmission and reflection amplitudes versus frequency are shown in Fig. 3 for eight states of phases when the y-polarized wave is considered as the incident wave. The simulations are accomplished by CST software with the periodic boundary conditions in the x- and y-directions and open space in the -z and +z-directions. It is clear that the x-polarized transmission coefficient is larger than 0.9 for states of 1,2,3, and larger than 0.56 for state of 4 in the working frequency band.

Table 1. Design parameters of the proposed unit cell.

Parameter	r_1	r_2	t_1	t_2	t_3	t_4	t_5
value [mm]	3.2	1.6	1.4	0.4	1	0.9	0.4
Parameter	p	α_1	α_2	β	H_1	H_2	h
value [mm]	6.5	8 states	8 states	8 states	1.57	1.57	0.038

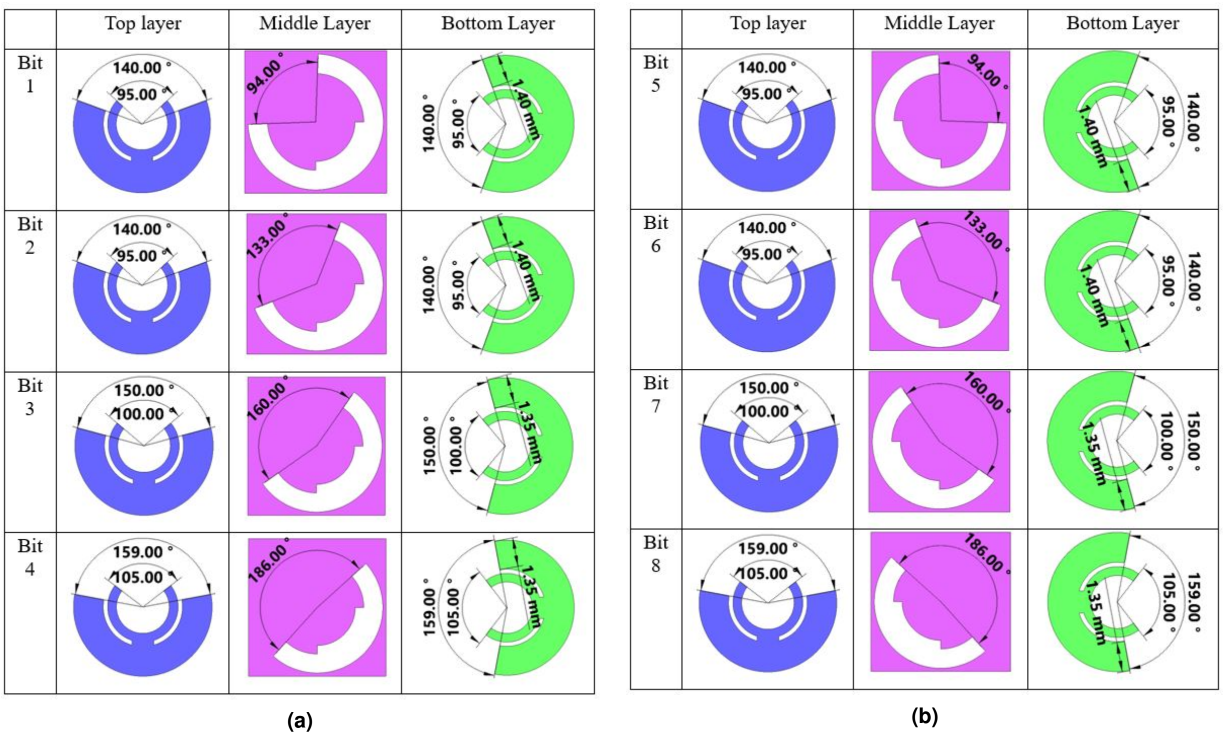

Figure 2. (a) Four states to provide transmission phases of 130°, 175°, 220°, 265°. (b) Four states to provide transmission phases of 310°, 355°, 40°, 85°.

Similar results are obtained for states of 5 to 8 which are not shown here. In order to clear the phase behavior of the element when the middle and bottom layers are rotated for making the states of 5 to 8, a full-wave simulation is done and the electric field distribution over these surfaces is investigated. The electric field distribution on the middle and bottom layers of states of 1 and 5 at 14 GHz are depicted in Fig. 4. A 180° phase difference between the states of 1 and 5 could be clearly observed from the direction of the electric fields on the bottom layers which are opposite to each other. The phase response of all 8 states versus frequency is also shown in Fig. 5. All phase responses are relatively linear behavior up to 16.5 GHz. Those states that have a phase difference of 180° to each other are shown with the same color. To summarize, the amplitude and phase of transmission wave for all 8 states are shown in Fig. 6 at the center and extreme frequencies of the band.

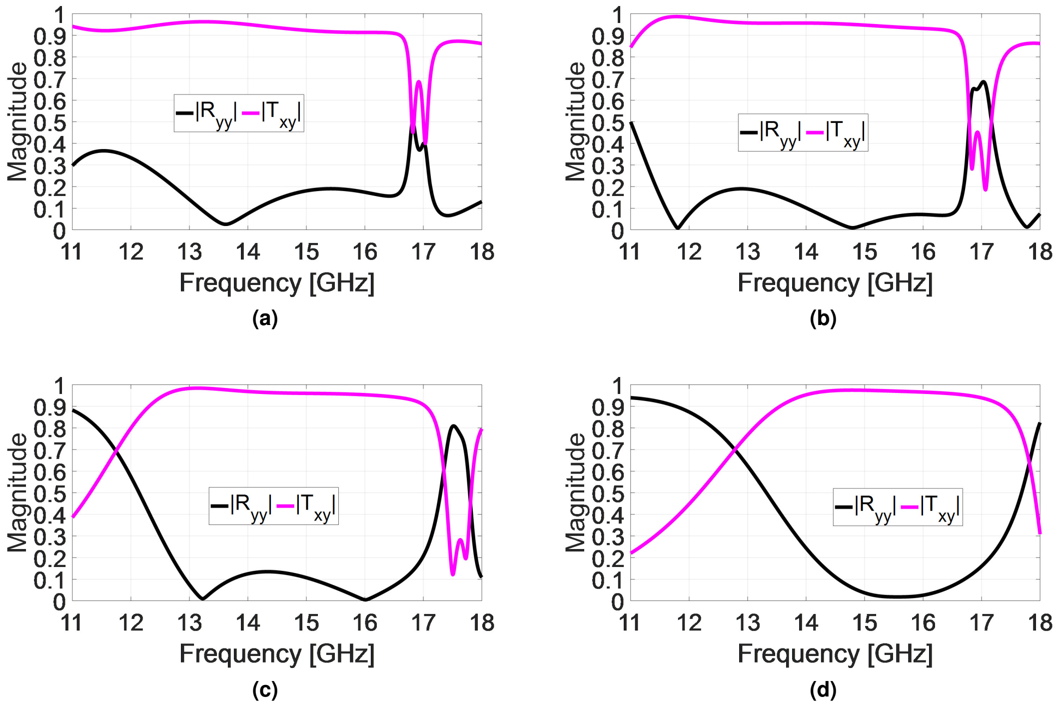

Figure 3. (a) Transmission and reflection coefficients for the y-polarized incident wave (a) state 1, (b) state 2, (c) state 3 (d) state 4.

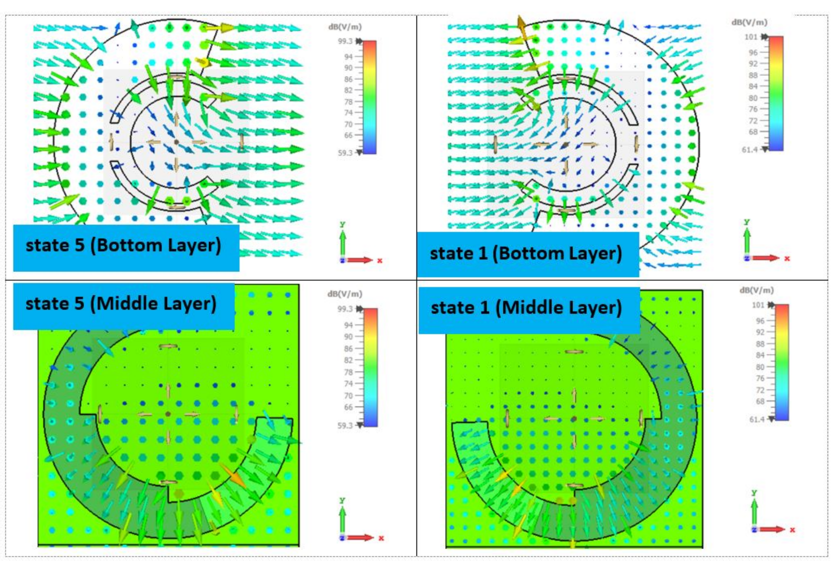

Figure 4. Electric field distribution on the middle and bottom layers associated with the states of 1 and 5 at 14 GHz.

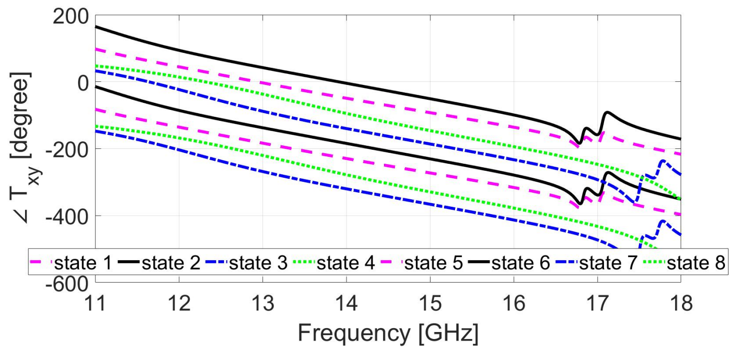

Figure 5. The phase response of all 8 states from 11 GHz to 18 GHz.

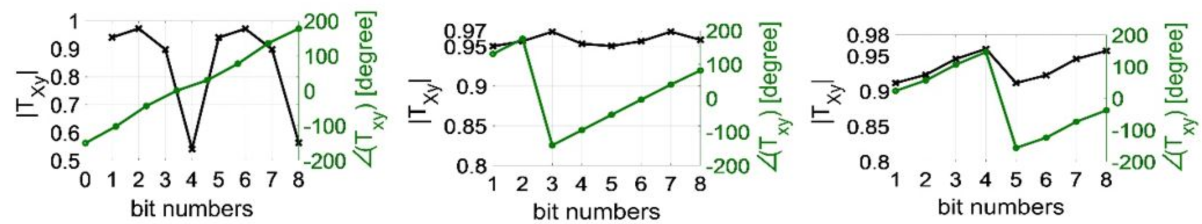

(a) (b) (c)

Figure 6. Amplitude and phase of transmission coefficients of all 8 states at 12.3 GHz, (b) 14 GHz, and (c) 16.5 GHz.

MFPS approach for 3-bit TFM

The MFPS approach, which is introduced by[24] along with the studies that followed to design broadband RFM[3,22], is employed in this paper for optimizing the phase distribution on the aperture to balance the overall phase error in all the band due to 3-bit phase quantization. The frequency band is initially considered from 12.3 GHz to 16.5 GHz, which is selected based on the element amplitude and phase behavior for all bits. In doing that, a global search algorithm based on particle swarm optimization (PSO) is utilized to balance the phase error in the frequency band and provide an optimum phase distribution for the TFM. The total phase error of all elements on the aperture along with the gain variance is considered as the cost function in the PSO. Several strategies have been employed at the system design level during the implementation of MFPS to achieve the best performance in terms of bandwidth and efficiency, which are discussed in the following: (i) the use of full-wave simulation results of the amplitude and phase of the horn field over the aperture; (ii) the use of full-wave simulation results for the amplitude of the transmission coefficient from the unit cell in all of the frequencies where the optimization is performed. This is done by considering the required phase and the corresponding state number based on the Fig. 3; (iii) the use of a horn with a relatively stable phase center with a symmetric radiation pattern and using the average of the simulated phase centers in the entire band to get the optimum position for the horn; (iv) Choosing the frequency at the beginning of the band, i.e., 12.3 GHz as the reference point in the optimization routine with the highest weighting factor to get the minimum possible phase error. This is why, in an ideal single-frequency phase synthesis approach, the curve of gain versus frequency has ascended behavior, therefore, the flat gain response is accessible if more phase errors would be forced at the end of the band than the frequencies at the beginning of the band. The required phase to transform a spherical incident wave to a planar wave focusing on (θ_b, ϕ_b), is determined as follows:

$$\varphi_{mn}^{req}(f) = \varphi_{\mathbf{0}}(f) + \frac{2\pi c}{f}\left(\varphi_{feed}(f) - x_{mn}\sin\theta_b\cos\phi_b - y_{mn}\sin\theta_b\sin\phi_b\right) \quad (1)$$

In (1), $\varphi_{feed}(f)$ is the phase of the electric field of the horn on the aperture which is extracted from CST software at the frequency f, $\varphi_{\mathbf{0}}(f)$ is the constant reference phase at f, x_{mn}, and y_{mn} are the position of the unit cells on the aperture plane.

In the MFPS approach, the constant reference phase is tuned within the frequency band of interest to minimize the overall phase error for all unit cells. The summation of phase errors relating to all unit cells as well as the variance of the gain in all frequencies of optimization are considered as the cost function as follows:

$$COST = \sum_{f_i} \left[w_{f_i} \sum_m \sum_n M_{mn,bit}(f_i) . P_{mn}(f_i) \right] + \mathrm{var}\left[G(f_i)\right], \; P_{mn}(f_i) = \left| \varphi_{mn}^{req}(f_i) - \varphi_{mn}^{achievable}(f_i) \right| \tag{2}$$

In (2), f_i is considered 10 equispaced samples from 12.3 to 16.5 GHz, P_{mn} is the phase error, w_{f_i} is set as a decreasing arithmetic sequence of $[1, 0.9, 0.8, ..., 0.1]$, $\mathrm{var}[G(f_i)]$ is the variance of the metasurface gain values within the band for all particles in each iteration of PSO. The gain values are computed with an enhanced accuracy by applying the aforementioned considerations, (*i*) to (*iv*), and using the fast Fourier transform (FFT) technique to accelerate the algorithm[1]. As shown in (3), $M_{mn,bit}(f_i)$ are coefficients depending on the illumination intensity which are obtained by multiplying the magnitude of the co-polarization field of the horn on the aperture, $\left|E_{mn}^{Horn,full-wave}(f_i)\right|$, and the magnitude of the transmission coefficient of the mn^{th} element ($\left|T_{mn,state}^{Element,full-wave}(f_i)\right|$). These two factors are extracted from CST software considering the state number of the element and the position of the element with respect to the horn antenna.

$$M_{mn,bit}(f_i) = \left|E_{mn}^{Horn,full-wave}(f_i)\right| \times \left|T_{mn,state}^{Element,full-wave}(f_i)\right| \tag{3}$$

Finaly, the achievable phase realized by the pratical coding surface is defined as follows:

$$\varphi_{mn}^{achievable} = \varphi_{bit} \quad if \; |\varphi_{bit} - \varphi_{mn}^{req}| < |\varphi_{bit}^{o.w} - \varphi_{mn}^{req}|, \; bit = 1, 2, ..., 8 \tag{4}$$

In (4), φ_{bit} is one of 8 states defined in Fig. 2 and $\varphi_{bit}^{o.w}$ is the phases other than φ_{bit} according to Fig. 2.

A 25×25-element TFM is designed in Ku-band based on the proposed combined broadband technique as a proof of concept. A Ku-band tangential profiled smooth-wall horn with $q = 6.5$, which was employed in our previous work[3], is chosen as the feeding source. The number of particles and iterations are considered 250 and 1000, respectively, to guarantee the convergence of the algorithm. The final optimum constant reference phases are obtained as $[-26, -80, 67, 114, -177, -158, -47, -26, -78, 81]$ degrees corresponding to 10 samples of frequencies.

Results and Discussion

Based on the criteria mentioned in the previous section, the optimal phase distribution of the TFM is obtained which is shown in Fig. 7a. By mapping the 8 phase states of the element represented in Fig. 2 to the phase distribution of Fig. 7a, the final arrangement of the elements in array environment is obtained for all three layers. Finally, the designed TFM and the feeding source (a smooth-wall conical horn antenna which was described in the previous section) was simulated by the time domain solver of the CST software installed on a computer system with 64G RAM. The feeding source is positioned in front of the TFM by considering the average phase center value versus the frequency in the working band. The simulation time for the designed TFM with dimensions of 16.5mm × 165.5 mm took about 8 hours.

The simulation results including the S11 parameter and 3D radiation pattern of TFM at 14 GHz are demonstrated Fig. 7b and Fig. 7c. The simulated 3D pattern shows the acceptable performance of the designed TFM in concentrating the wave emitted from the horn. The simulated peak gain at 14 GHz is 25.8 dBi, which corresponds to an aperture efficiency of 52.6%. In addition, the S11 of the structure defined from the input port of the horn as the feeding source is below -20 dB which is acceptable. This shows that most of the wave passes through the TFM, which is predictable based on the simulation results presented in Fig. 3.

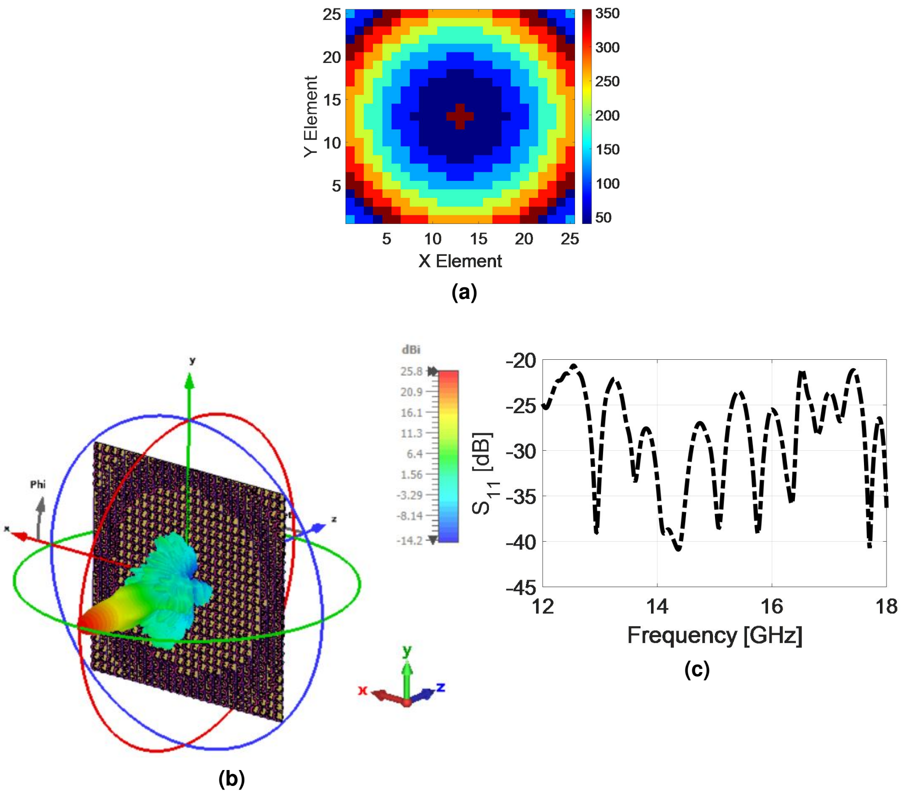

Figure 7. (a) Optimal phase distribution at 14 GHz to achieve a broadband high-efficiency TFM (b) 3D demonstration of absolute gain of the designed TFM at 14 GHz. (c) Simulated S11 of TFM.

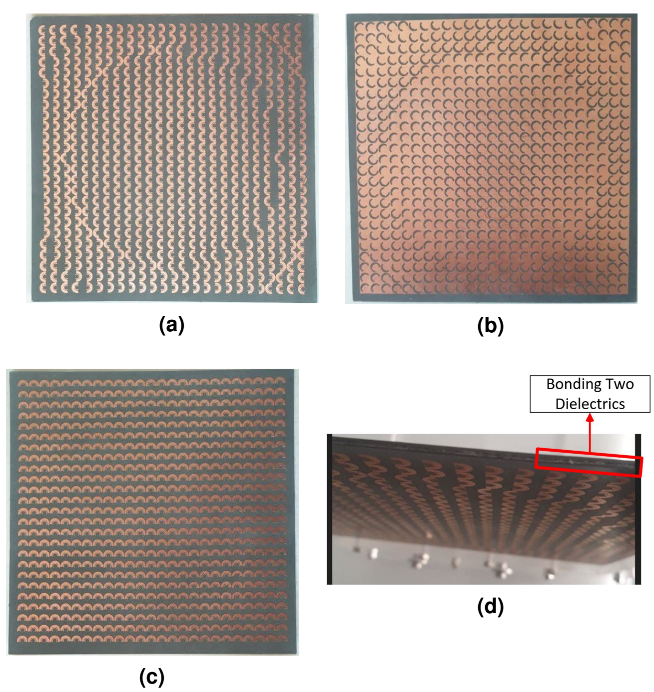

Figure 8. Fabricated two layers of TFM. (a) Front view of the top layer. (b) Back view of the top layer. (c) Front view of the bottom layer. (d) Close view from the bonding region of the two dielectrics.

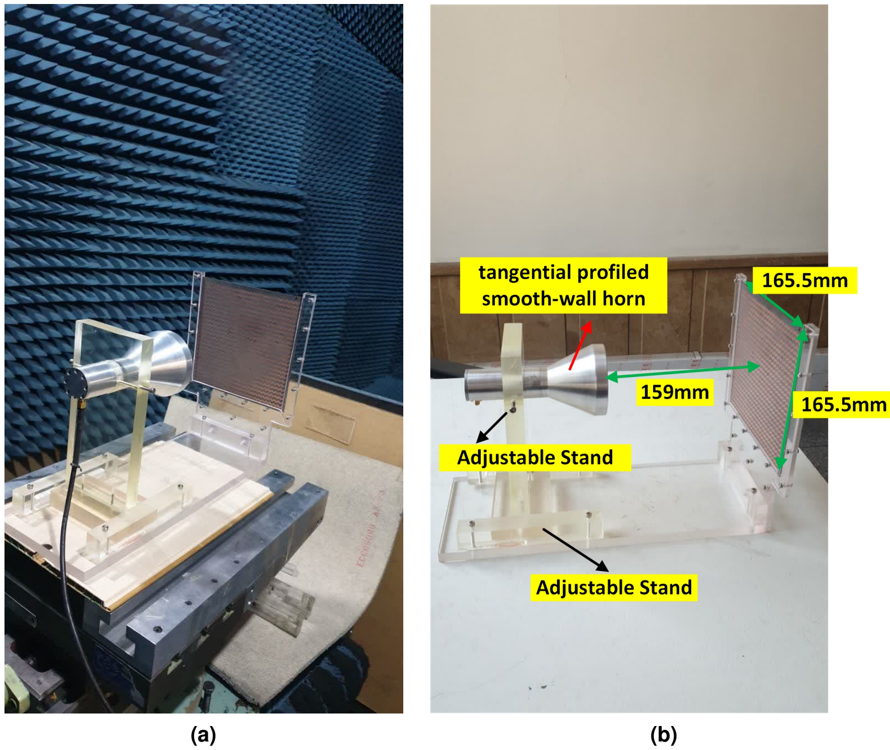

Figure 9. Measurement setup in an anechoinc chamber.

In order to experimentally validate the designed broadband high-efficiency TFM, a prototype was fabricated based on the printed circuit board (PCB) technology. The fabricated metasurface and measurement setup are demonstrated in Fig. 8 and 9. In order to fix the position of the feed with respect to the TFM, we used a setup made up of plexiglass with a flexible focal length. A strong frame is considered around the TFM and fixed it with some plastic screws. The far-field radiation patterns are measured at the center and extreme frequencies of the band in an anechoic chamber. Figure. 10 compares the simulated and measured far-field patterns in the E- and H-planes, which show good consistency between them. The measurement results show that the side lobe levels are below -20 dB for all three frequency points in both planes and the cross-polarization component of the pattern is below -28 dB at all angles. It is worth mentioning that the designed unit cell element has a similar electromagnetic behavior when the wave is illuminated to the aperture in the opposite direction (-z-direction) with orthogonal polarization. Therefore, it is expected that if the horn is positioned on another side of the TA with the same f/D, and rotated by 90° around its longitudinal axis, in this scenario, the transmitted wave also has similar characteristics as the results shown in Fig. 10. The measured 1-dB gain bandwidth and the corresponding aperture efficiency of the proposed metasurface are demonstrated in Fig. 11. The results show that the maximum realized gain is 25.8 dB. Furthermore, the maximum aperture efficiency is measured at 12.8 GHz, which equals to 53.6%. To show the advantage of using the MFPS approach integrating with multi-bit coding metasurface concept to simultaneously improve the bandwidth and efficiency of TFM, we designed two other TFMs. The first one is designed based on the classic single-frequency phase synthesis approach, in which the phase error becomes minimum at only one frequency which is called *design frequency*. The second one is a single-bit TFM with two states for the phase distribution, (state of 3 and 6 in Fig. 2 for example), in which the MFPS approach is also employed. The simulation results of the peak gain versus the frequency are shown in Fig. 11.

The comparison of the peak gains shows that the use of single-bit TFM has a wider 1-dB bandwidth in comparison with the other two radiators, that is, from 12.7 GHz to 17.5 GHz, however, the maximum gain of this metasurface is nearly 2 dB lower than the 3-bit configuration which in turn causes to lower aperture efficiency.

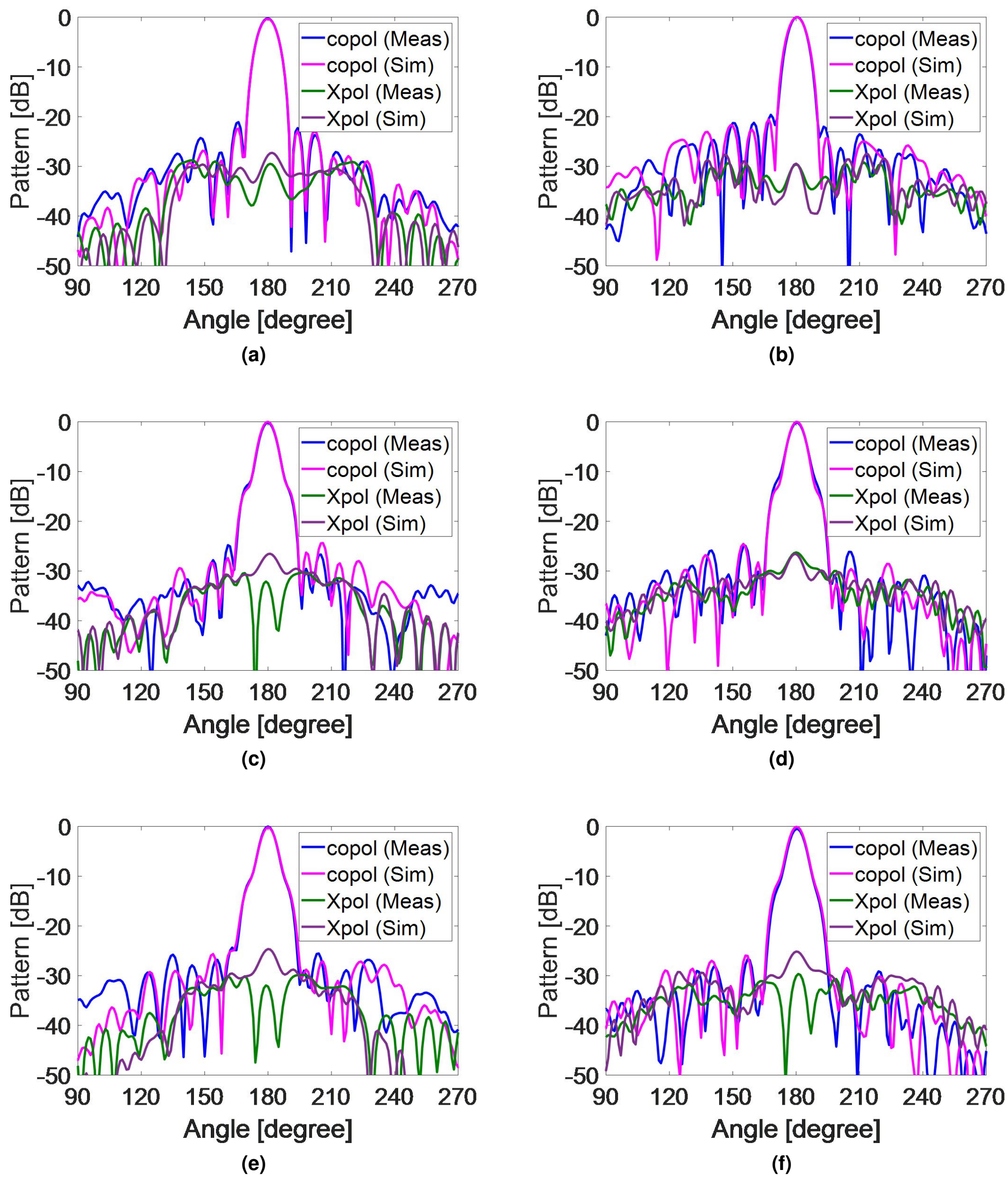

Figure 10. Simulation and measurement results of the normalized gain in the E- and H-planes (a) E-plane at 12.3 GHz, (b) H-plane at 12.3 GHz, (c) E-plane at 14 GHz, (d) H-plane at 14 GHz, (e) E-plane at 16.5 GHz, (f) H-plane at 16.5 GHz.

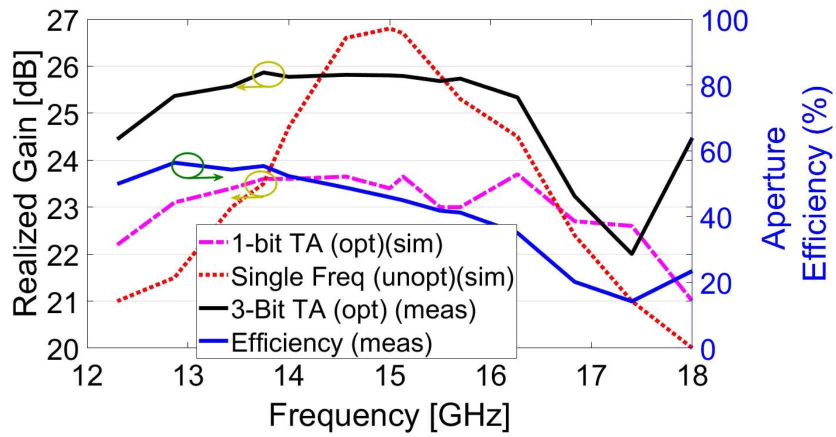

Figure 11. Comparison between different scenarios to design a TFM along with the measured aperture efficiency. "opt" and "unopt" stands for the optimized and unoptimized model, respectively.

In addition, the side lobe levels in single-bit coding TFM are obtained at about -17dB for all frequencies of optimizations, which are higher than side lobe levels in 3-bit TFM. This is why the phase distribution in multi-bit configurations would be closer to the ideal phase distribution which is dictated by the ray tracing theory in space-fed metasurfaces. In the second simulation, the design frequency is considered 15 GHz. It is clear from Fig. 11 that the minimum phase error occurs at 15 GHz. The maximum peak gain of singe-frequency TFM is obtained to be 26.9 dB, which is around 1.2 dB higher than the 3-bit TFM, this is why the phase error in the MFPS approach is balanced, and not the minimum value, within the band to achieve a gentler gain response. A comparison is done between the performance of the presented work and the previously published works which are represented in Table. 2. The comparison shows that the presented TFM has a high aperture efficiency and 1-dB gain bandwidth at the same time thanks to the use of combined broadband technique integrating with multi-bit coding metasurface.

Table 2. Comparison of the proposed 3-bit wideband high-efficiency TFM with other works.

Ref. Number	**This work**	Ref.[25]	Ref.[26]	Ref.[27]	Ref.[28]	Ref.[29]
Freq [GHz]	**14**	10	15	27	8.5	150
Via	**No**	No	No	Yes	Yes	No
Technology	**PCB**	PCB	PCB	PCB	Metal Only	PCB
Phase. Dist	**3-Bit**	2-Bit	Continuous	1-Bit	1-Bit	six states
Dielectric. Num	**2**	2	3	4	2	2
Max. AE	**53.4%**	17%	42.3 %	28 %	47.6 %	32 %
1-dB Gain	**%29**	33.4 % (3-dB)	37.3 %	N. A	14.6 %	16.8 %
Fabrication	**Easy**	Easy	Easy	Difficult	Difficult	Easy
Thickness	**$0.14\lambda_0$**	$0.05\lambda_0$	$0.165\lambda_0$	$0.16\lambda_0$	$0.23\lambda_0$	$0.25\lambda_0$

Conclution

A novel broadband high-efficiency coding metasurface in transmissive mode is designed, fabricated, and tested in this paper. By integrating the multi-bit configuration and MFPS approach from the gain level point of view, the phase error reached to its minimum possible value in the frequency band such that the gain has a flat response. In doing so, the priority is to minimize the phase errors at the beginning frequencies of the band, since the gain curve versus the frequency is ascending, therefore, the gentle gain response is merely realizable If we force more phase error at the frequencies of the end of the band. The 1-dB gain bandwidth of the designed metasurface is 29% and the maximum aperture efficiency is obtained 53.6%.

References

1. Nayeri, P., Yang, F. & Elsherbeni, A. Z. Reflectarray antennas: theory, designs, and applications. (2018).

2. Abdelrahman, A. H., Yang, F., Elsherbeni, A. Z. & Nayeri, P. Analysis and design of transmitarray antennas. *Synth. Lect. on Antennas* **6**, 1–175 (2017).
3. Karimipour, M. & Aryanian, I. High-efficiency dual-polarized broadband reflecting metasurface using continuous polarization conversion technique and element with multi degree of freedom. *Sci. Reports* **12**, 1–13 (2022).
4. Deng, R., Xu, S., Yang, F. & Li, M. A single-layer high-efficiency wideband reflectarray using hybrid design approach. *IEEE Antennas Wirel. Propag. Lett.* **16**, 884–887 (2016).
5. Karimipour, M. & Aryanian, I. Demonstration of broadband reflectarray using unit cells with spline-shaped geometry. *IEEE Transactions on Antennas Propag.* **67**, 3831–3838 (2019).
6. Tian, C., Jiao, Y.-C., Zhao, G. & Wang, H. A wideband transmitarray using triple-layer elements combined with cross slots and double square rings. *IEEE Antennas Wirel. Propag. Lett.* **16**, 1561–1564 (2017).
7. Hsu, C.-Y. *et al.* Transmitarray design with enhanced aperture efficiency using small frequency selective surface cells and discrete jones matrix analysis. *IEEE Transactions on Antennas Propag.* **66**, 3983–3994 (2018).
8. Wang, X., Cheng, Y. & Dong, Y. Millimeter-wave high-efficiency double-layer transmitarray antenna using miniaturized dual-polarized elements. *IEEE Transactions on Antennas Propag.* (2022).
9. Feng, P.-Y., Qu, S.-W. & Yang, S. Octave bandwidth transmitarrays with a flat gain. *IEEE Transactions on Antennas Propag.* **66**, 5231–5238 (2018).
10. Rahmati, B. & Hassani, H. High-efficient wideband slot transmitarray antenna. *IEEE Transactions on Antennas Propag.* **63**, 5149–5155 (2015).
11. An, W., Xu, S., Yang, F. & Li, M. A double-layer transmitarray antenna using malta crosses with vias. *IEEE transactions on antennas propagation* **64**, 1120–1125 (2015).
12. Abdelrahman, A. H., Nayeri, P., Elsherbeni, A. Z. & Yang, F. Bandwidth improvement methods of transmitarray antennas. *IEEE Transactions on Antennas Propag.* **63**, 2946–2954 (2015).
13. Mei, P., Pedersen, G. F. & Zhang, S. A broadband and fss-based transmitarray antenna for 5g millimeter-wave applications. *IEEE Antennas Wirel. Propag. Lett.* **20**, 103–107 (2020).
14. Li, M., Al-Joumayly, M. A. & Behdad, N. Broadband true-time-delay microwave lenses based on miniaturized element frequency selective surfaces. *IEEE transactions on antennas propagation* **61**, 1166–1179 (2012).
15. Cao, Y., Yang, W., Xue, Q. & Che, W. A broadband low-profile transmitarray antenna by using differentially driven transmission polarizer with true-time delay. *IEEE Transactions on Antennas Propag.* **70**, 1529–1534 (2021).
16. Lei, H., Liu, Y., Jia, Y., Yue, Z. & Wang, X. A low-profile dual-band dual-circularly polarized folded transmitarray antenna with independent beam control. *IEEE Transactions on Antennas Propag.* **70**, 3852–3857 (2021).
17. Derafshi, I. & Komjani, N. A new high aperture efficiency transmitarray antenna based on huygens metasurfaces. *IEEE Transactions on Antennas Propag.* (2022).
18. Wu, L. W. *et al.* High-transmission ultrathin huygens' metasurface with 360 phase control by using double-layer transmitarray elements. *Phys. Rev. Appl.* **12**, 024012 (2019).
19. Wang, X., Cheng, Y. & Dong, Y. Millimeter-wave dual-polarized metal transmitarray antenna with wide gain bandwidth. *IEEE Antennas Wirel. Propag. Lett.* **21**, 381–385 (2021).
20. Yu, W., Wang, Y., Deng, F. & Lin, H. Broadband 1-bit dual-polarized metasurface-based reflectarray antenna with beams control. In *2021 IEEE International Workshop on Electromagnetics: Applications and Student Innovation Competition (iWEM)*, 1–3 (IEEE, 2021).
21. Yu, S., Li, L. & Kou, N. One-bit digital coding broadband reflectarray based on fuzzy phase control. *IEEE Antennas Wirel. Propag. Lett.* **16**, 1524–1527 (2017).
22. Liu, S., Sato, H. & Chen, Q. A wideband, 1 bit transmitarray antenna design with flat gain response. *IEEE Transactions on Antennas Propag.* **68**, 7046–7055 (2020).
23. Koutsos, O., Manzillo, F. F., Clemente, A. & Sauleau, R. Analysis, rigorous design, and characterization of a three-layer anisotropic transmitarray at 300 ghz. *IEEE Transactions on Antennas Propag.* **70**, 5437–5446 (2022).
24. Mao, Y., Xu, S., Yang, F. & Elsherbeni, A. Z. A novel phase synthesis approach for wideband reflectarray design. *IEEE transactions on antennas propagation* **63**, 4189–4193 (2015).

25. Mavrakakis, K., Luyen, H., Booske, J. H. & Behdad, N. Wideband transmitarrays based on polarization-rotating miniaturized-element frequency selective surfaces. *IEEE Transactions on Antennas Propag.* **68**, 2128–2137 (2019).

26. Li, M.-Y., Ban, Y.-L. & Yan, F.-Q. Wideband low-profile ku-band transmitarray antenna. *IEEE Access* **9**, 6683–6688 (2020).

27. Wu, F. *et al.* Wideband and low cross-polarization transmitarray using 1 bit magnetoelectric dipole elements. *IEEE Transactions on Antennas Propag.* **69**, 2605–2614 (2020).

28. Hu, W. *et al.* A wideband metal-only transmitarray with two-layer configuration. *IEEE Antennas Wirel. Propag. Lett.* **20**, 1347–1351 (2021).

29. Saleh, W., Letestu, Y., Sauleau, R. & Cruz, E. M. Design and measurements of a high-performance wideband transmitarray antenna for d-band communications. *IEEE Antennas Wirel. Propag. Lett.* **20**, 1765–1769 (2021).

Acknowledgements

The authors would like to thank from Iran Telecommunication Research Center (ITRC) for providing the RF laminate and testing the prototype.

Author contributions statement

Dr. M. Karimipour proposed the main idea of this work. The simulations and writing the paper are also done by Dr. M. Karimipour. and Dr. M.B. Heydari. Dr. I. Aryanian conducted the experiments, analyzed the results, and review the paper.

Competing interests

The authors declare no competing interests.